

Complex pathways and memory in compressed corrugated sheets.

Hadrien Bense*

AMOLF, Science Park 104, 1098 XG Amsterdam, The Netherlands

Martin van Hecke†

*AMOLF, Science Park 104, 1098 XG Amsterdam, The Netherlands and
Huygens-Kamerlingh Onnes Lab, Leiden University, PObox 9504, 2300 RA Leiden, The Netherlands*

(Dated: April 17, 2022)

The nonlinear response of driven complex materials—disordered magnets, amorphous media, crumpled sheets—features intricate transition pathways where the system repeatedly hops between metastable states. Such pathways encode memory effects and may allow information processing—yet tools are lacking to experimentally observe and control these pathways, and their full breadth has not been explored. Here we introduce compression of corrugated elastic sheets to precisely observe and manipulate their full, multi-step pathways, which are reproducible, robust, and controlled by geometry. We show how manipulation of the boundaries allows to elicit multiple targeted pathways from a single sample. In all cases, each state in the pathway can be encoded by the binary state of material ‘bits’ called hysterons, and the strength of their interactions plays a crucial role. In particular, as function of increasing interaction strength, we observe Preisach pathways, expected in systems of independently switching hysterons, ‘scrambled’ pathways that evidence hitherto unexplored interactions between these material bits, and ‘accumulator’ pathways which leverage these interactions to perform an elementary computation. Our work opens a route to probe, manipulate and understand complex pathways, impacting future applications in soft robotics and information processing in materials.

The response of complex media to external driving is intermittent, featuring smooth reversible episodes, associated with a single (meta)stable state of the system, punctuated by sharp irreversible steps between states that together form a multi-step pathway [1–7]. These steps are hysteretic, and the ensuing complex pathways are often modeled by collections of hysteretic, two-state elements called *hysterons* [8]. These two-state hysteretic elements switch up and down between internal states $s = 0$ and $s = 1$ when a driving field U passes through the upper and lower switching fields U^+ or U^- (with $U^+ > U^-$); the state of the hysteron for $U^- \leq U \leq U^+$ depends on its driving history. One can think of these as ‘material bits’ [9–11] that collectively label the (meso)state of the physical system. Properties such as memory are then determined by the sequences of bit switches as function of a global driving U , which can be encoded in so-called transition graphs, whose nodes represent the mesostates and edges their transitions [12, 13].

Collections of uncoupled n hysterons form the Preisach model [8], which has been studied extensively in the context of complex hysteresis and memory effects. The absence of coupling implies that hysteron i changes state at switching fields U_i^+ and U_i^- which are independent of the state of the other hysterons. As a result, the sequence of bit switches in response to sweeping U is given by the ordering of the $2n$ switching fields. This restricts the type of pathways that are possible, with the transition graphs featuring a hierarchical structure of loops within loops.

Finally, this model exhibits return point memory (RPM), the widespread ability of complex systems to ‘remember their extremal driving’, i.e., to return to a previous state when the driving revisits an extremum [14–18].

Recently, simulations of models of coupled hysterons as well as amorphous media have found evidence for complex pathways and transition graphs featuring, e.g., avalanches, multiple memories and multi-periodic orbits, which cannot be captured by models of non-interacting hysterons [5, 19, 20]. Unfortunately, distinguishing, observing and manipulating individual hysterons and their interactions is challenging for most complex systems. Hence the connection between hysteron models and experimentally observable pathways, as well as the relevance of hysteron interactions for driven complex media, remains unclear. As a result, we do not understand the effect and importance of hysteron interactions on the pathways and memory in driven complex media.

Here we introduce mechanical compression of curved, corrugated elastic sheets to directly observe mechanical hysterons, their interactions and their concomitant non-trivial pathways (Fig. 1). We find that, due to interactions, the driving value where a given hysteron switches is modified by the states of the other hysterons. As a consequence, the precise values of the driving where a given hysteron switches state become state-dependent, $U_i^\pm(\mathbf{S})$, which can lead to a breakdown of strict return point memory. For increased interactions, the switching order of the hysterons can become state dependent, allowing a multitude of more complex bit-switching sequences. Specifically, the hierarchical loop-within-loop structure of hysteresis cycles can be broken, bringing sequences of bit flips that encode forms of information processing within

* hbense.h@gmail.com

† m.v.Hecke@amolf.nl

reach, creating new opportunities for soft robotics [21–24] and information processing in materials [9–11, 25].

I. RESULTS AND DISCUSSION

A. Mechanical hysterons with robust pathways

In our design, the corrugations lead to spatially localized instabilities upon compression which act as mechanical hysterons, the overall curvature prevents global buckling of the sheet, and the open cylindrical structure allows to limit the number of grooves and facilitates both observation and manufacture. Our experimental protocol involves sweeping the axial compression of a groovy sheet while filming the sample and measuring the compressive force F (Fig. 1a-e; see Methods and Supplementary Movies). We observe that our samples exhibit sequences of well-defined steps, seen as sharp jumps in the force F , and find that each event is associated with a localized (un)snapping event in a vertical groove, similar to those seen in tape springs [26] (Fig. 1c-e, Methods and Supplementary Movies). These transitions are hysteretic and we observe that each groove can be in two distinct states—snapped and unsnapped—so that each groove acts as a mechanical hysteron. We refer to the hysteron transitions as ‘up’ (from the unsnapped to the snapped state) and ‘down’ (snapped to unsnapped), and denote the corresponding compression thresholds by the switching fields U^+ and U^- (Fig. 1f-h).

Repeated compression loops yield highly reproducible pathways with virtually identical force curves and sequences of hysteron-flipping, evidencing the irrelevance of creep, plasticity or aging (see Supplementary Information). A wide range of groovy cylinders responds similarly to cyclical compression, and while we focus on systems with three grooves/hysterons, which is the minimal number for complex pathways, we have observed similar phenomena in larger systems (see Supplementary Information). As we will show below, modifications of the sheet’s shape and boundary conditions allow to geometrically tune the properties and interactions of their hysterons, making this system a viable platform to study reproducible, directly observable, and tunable pathways.

B. Pathways and transition graphs

We map the full pathway by submitting the sample to a series of well-chosen compression/decompression cycles (Fig. 1i). Different driving cycles induce different pathways, which together form an intricate web of linked hysteresis loops [14, 15] which connect distinct states. These states and their transitions can be collected into a transition graph (t-graph), a directed graph that captures the response to *any* sequence of increases and decreases of the global driving field U [4, 5, 12, 13, 19, 27, 28]. To experimentally map the t-graph we systematically visit

all states and determine all transitions, while tracking the state of each hysteron s_i , where $s_i = 1$ (0) refers to a snapped (unsnapped) state. A state \mathbf{S} is characterized by the hysteron states $\{s_1, s_2, \dots\}$. For each state—with the exception of the ground state $\{0\dots 0\}$ and saturated state $\{1\dots 1\}$ —increased or decreased compression yields ‘up’ and ‘down’ transitions at critical switching fields $U_i^+(S)$ and $U_i^-(S)$. To determine all transitions, we first determine the main loop, the sequence of transitions that, under monotonic compression or decompression, connect the ground state and saturated state [13]. We then check whether there are states for which there are undetermined transitions, determine these, and whenever we obtain a state that has not been previously visited we also determine its transitions, repeating these operations until no new states are found. Collecting all states and transitions we obtain the t-graph in which the nodes represent the mesostates, and the directed edges, labeled by the values of their respective switching fields, the transitions (Fig. 1j).

For the simple case shown in Fig. 1i-j, starting out at the uncompressed state $\{000\}$ and monitoring the force and images, we find that continued compression yields a sequence $\{000\} \rightarrow \{001\} \rightarrow \{011\} \rightarrow \{111\}$; decompression starting at the saturated state yields a sequence $\{111\} \rightarrow \{011\} \rightarrow \{001\} \rightarrow \{000\}$. For this specific example, a simple compression/decompression cycle (Fig. 1d) is enough to obtain the full set of transitions. A more complex protocol (inset of Fig. 1i) yields a force response with three nested hysteresis loops (Fig. 1i) that illustrates the different pathways the system can follow, and hence the importance of the loading history. The corresponding t-graph also features three sub-loops embedded in the main loop and is span by four nodes and six edges; the material bits simply switch on and off when the driving is swept up and down.

C. Tunable pathways

A wide variety of more complex t-graphs can be observed by tilting one of the boundaries of the sample (Fig. 1b, Fig. 2a-b, see Methods). Due to the spatial separation of each hysteron, applying such global gradients in the driving modifies the relation between global and local compression, leading to the smooth tuning of the switching fields U_i^\pm (Fig. 3a and Supplementary Information). As the relative order of the switching fields determines the order in which hysterons flip, tilting allows to visit different states and/or sequences, thus modifying the topology of the t-graphs. By sweeping α , we observe seven distinct responses in sample A (Fig. 2a). We characterize the order of the switching fields of the main loop by the corresponding sequence of hysteron flips, P^+ and P^- (Fig. 2a). For example, in the main loop of sample A in regime (ii), the second hysteron flips first ($\{000\} \rightarrow \{010\}$), followed by the third hysteron ($\{010\} \rightarrow \{011\}$) and finally the first one ($\{011\} \rightarrow \{111\}$),

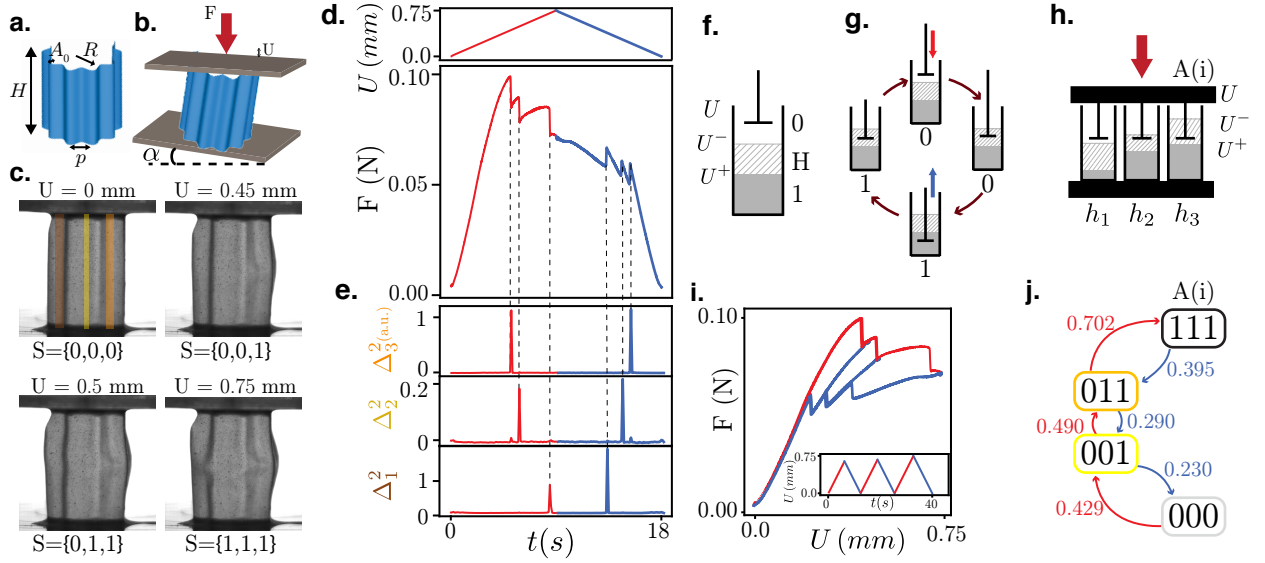


FIG. 1. **Robust pathways in a cyclically compressed corrugated sheet.** **a**, Our samples are corrugated elastic cylindrical shells of height H , thickness t , radius of curvature R , and N sinusoidal corrugations of pitch p and amplitude A_0 . For sample A, shown here, $N = 3$ and $\{H, t, R, p, A_0\} = \{35, 0.2, 1.0, 8, 3\}$ mm. **b**, Compression U , force F and bottom plate tilt angle α . **c**, Upon compression at $\alpha = 0$ mrad, sample A reaches four different mesostates, associated with sudden snapping of distinct regions Ω_i (colored strips, see Supplementary Movie). **d**, The force F exhibits three sharp jumps during compression (red) and decompression (blue). **e**, Each force jump is associated with a sudden deformation, evidenced by spikes in Δ_i^2 , the sum of the squared differences between subsequent digital images restricted to Ω_i (see Methods). **f**, Schematic representation of a hysteron, its state, and the switching fields U^\pm , where $U^- < U < U^+$ is the hysteretic range. **g**, Evolution of hysteron state during a compression cycle. **h**, Our samples behave as collections of parallel hysterons with distinct thresholds. **i**, Force-displacement curve corresponding to increasing compression cycles (inset). **j**, The transition graph of sample A at $\alpha = 0$ mrad contains four states (nodes) labeled by the state of each hysteron. Red (blue) arrows correspond to up (down) transitions at (de)compression U_c as indicated in mm.

yielding $P^+ = [2, 3, 1]$. Similarly, during decompression, the first hysteron unflips first ($\{111\} \rightarrow \{011\}$), then the second ($\{011\} \rightarrow \{001\}$) and finally hysteron number three ($\{001\} \rightarrow \{000\}$), leading to $P^- = [1, 2, 3]$. Many of the t-graphs exist on a large angle span, while others can only be observed for a limited range of tilt angles α (Fig. 2b). We note that during the tilting process, two switching fields can become extremely close, such that their respective (un)snapping events become indistinguishable (e.g., in Fig. 1b the two data points between A(ii) and A(iii) refer to such a case). This degeneracy may cause an avalanche. However, we can distinguish degeneracy-driven avalanches from true avalanches by their response to changes in the tilt angle: degeneracy-driven avalanches quickly disappear when the angle is modified, while true avalanches persist over a significant range of α .

We note that in most cases, the difference between neighboring t-graphs is associated with a single permutation of the upper or lower transitions; for example compare graph A(i), where $P^+ = [3, 2, 1]$ to A(ii) where $P^+ = [2, 3, 1]$ corresponding to a swap of the snapping order of hysterons 2 and 3. Such permutation is consistent with the notion that tilting smoothly tunes the switching fields. Plots of the switching fields directly evidence their smooth variation with the tilt angle α , and show that

the ranges of α where each t-graph occurs are consistent with the crossing of two switching fields; for example, the change from graph A(i) to A(ii) corresponds to the crossing of U_2^+ and U_3^+ (Fig. 3b and Supplementary Information). We have obtained a similar range of t-graphs for a sample B which contains four hysterons (see Supplementary Information). We conclude that global driving gradients are a powerful tool to systematically elicit a multitude of t-graphs from a single sample.

D. Preisach and scrambled t-graphs

A close inspection of the topology of the t-graphs of sample A reveals two distinct classes of graphs: Preisach graphs A(i), (ii), (iii), (v), (vi) and (vii) and scrambled graphs A(iv). To understand this distinction, consider the relation between the flipping of the individual hysterons and the state transitions. For n hysterons with states s_i , forming a collective state \mathbf{S} , the up (resp. down) transitions are set by the hysteron in state $s = 0$ (resp. $s = 1$) which has the lowest up (resp. highest down)

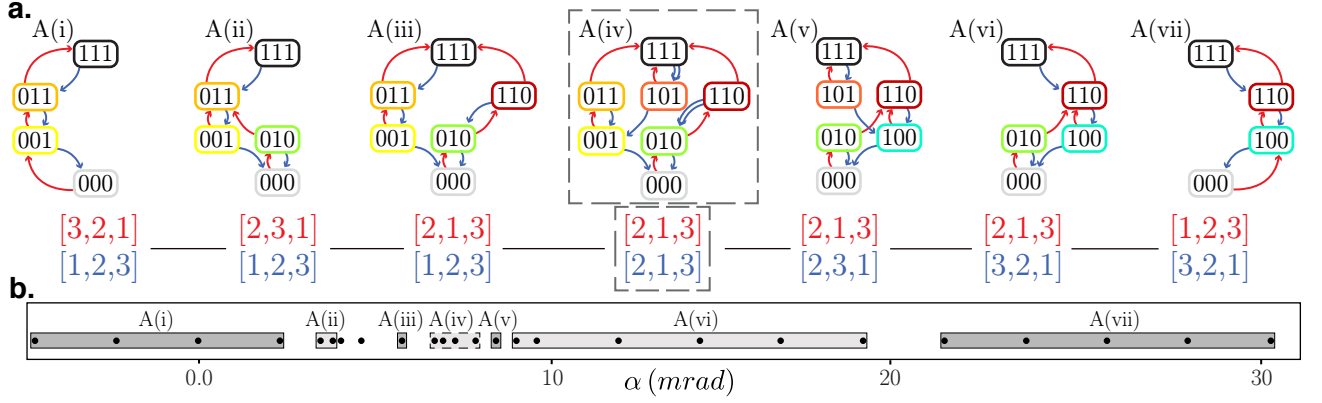


FIG. 2. **Tunable transition graphs.** **a**, Tilting the bottom boundary of sample A elicits six Preisach t-graphs and one scrambled t-graph (dashed box), where scrambled transitions are shown by double arrows. The red (blue) lists indicate the order of the up (down) transitions of the main loop P^+ (P^-). The angle α increases monotonically from $A(i)$ to $A(vii)$. **b**, t-graph type as function of α . The two unlabeled dots near $\alpha = 5$ mrad refer to ambiguous cases where the critical switching fields U_1^+ and U_3^+ are so close that the difference between type (ii) and (iii) is not experimentally significant.

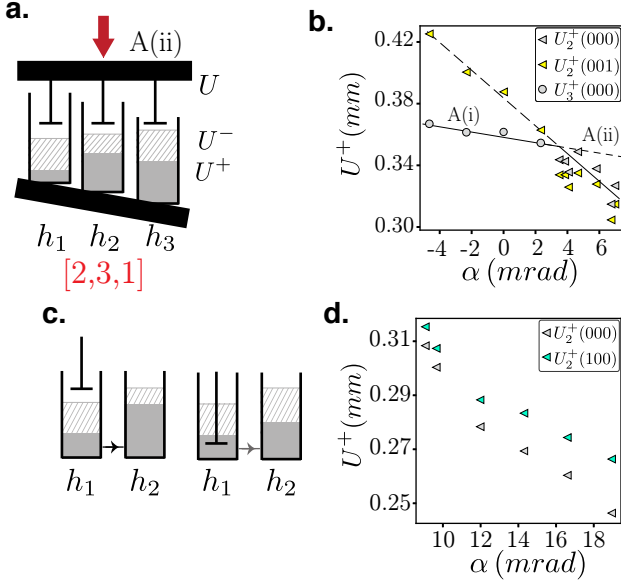


FIG. 3. **Change of pathway and interactions.** **a**, The boundary tilt modifies the relation between local and global compression U , and can reorder the switching fields as indicated. **b**, The switching fields vary smoothly with α , and the t-graph $A(i)$ is replaced by $A(ii)$ when $U_2^+(000)$ and $U_3^+(000)$ swap order. **c**, Interactions cause the state of a given hysteron to modify the switching fields of another hysteron; here hysteron 1 going $0 \rightarrow 1$ increases U_2^+ . **d**, The measured difference between $U_2^+(000)$ and $U_2^+(100)$ indicates hysteron interactions as in panel (c).

switching field:

$$U^+(\mathbf{S}) = \min_{i_0} u_{i_0}^+(\mathbf{S}), \quad (1)$$

$$U^-(\mathbf{S}) = \max_{i_1} u_{i_1}^-(\mathbf{S}). \quad (2)$$

Here i_0 (resp. i_1) runs over the hysterons that are in state 0 (resp. 1), $U^\pm(\mathbf{S})$ are the global switching fields for the collective states \mathbf{S} , and u_i^\pm are the state-dependent switching fields of individual hysterons.

In absence of hysteron interactions, the switching fields of all hysterons are independent of the state of the other hysterons ($u_i^\pm(\mathbf{S}) = u_i^\pm$), and the topology of the t-graph is thus fully determined by the ordering of the up and down switching fields of individual hysterons. We refer to t-graphs whose topology is consistent with a unique ordering of the upper and lower switching fields of the hysterons, and which do not contain avalanches, as Preisach graphs (recall that collections of non-interacting hysterons are referred to as the Preisach model [28]). We note that the topology of a Preisach graph is fully determined by the order of the transitions of the main loop, encoded in P^+ and P^- . We stress here that t-graphs with a Preisach topology do not require the strict absence of interactions, but only that interactions do not introduce differences between the ordering of the transitions in the main loop and the rest of the t-graph.

Strikingly, we also observe a *scrambled* graph which features pairs of transitions that are not consistent with a unique, state-independent ordering of the switching fields—we call these transitions scrambled. In particular, t-graph $A(iv)$ contains the pair of transitions $\{111\} \rightarrow \{101\}$ and $\{110\} \rightarrow \{010\}$, which is not compatible with a unique, state-independent ordering of the switching fields $U_2^- > U_1^-$; rather these transitions imply that $U_2^-(111) > U_1^-(111)$ and $U_2^-(110) < U_1^-(110)$ respectively (Fig. 2a). Such state-dependent ordering of the switching field is incompatible with a Preisach graph and demonstrates a dependence of the switching field of one hysteron on the state of another hysteron, thus directly evidencing hysteron interactions. Intuitively, scrambling implies that bit-flip sequences depend on the starting state, allowing for a far larger space of potential

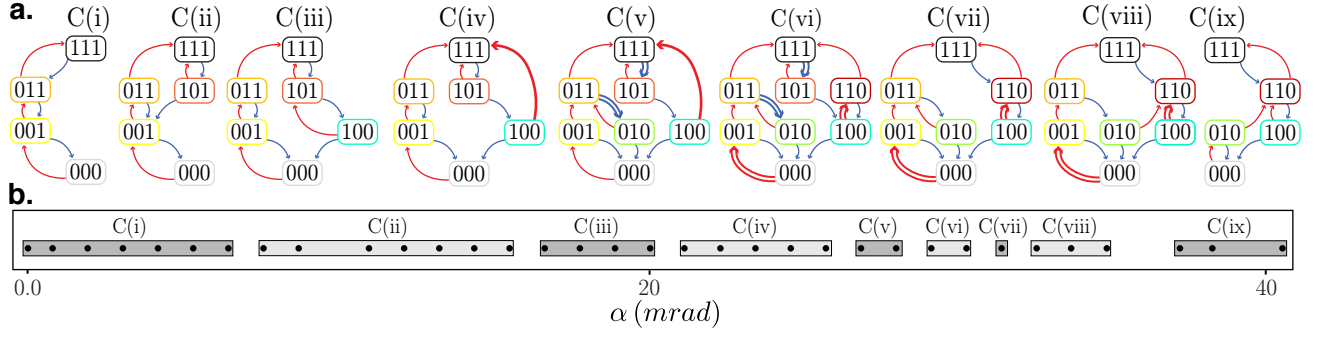


FIG. 4. **t-graphs of sample C.** **a**, Tilting sample C ($\{H, t, R, p, A_0\} = \{20, 0.2, 2.0, 10, 3\}$) mm and $N = 3$ corrugations) elicits nine distinct t-graphs. **b**, t-graph type as a function of α .

t-graphs than Preisach graphs. Additional evidence of interactions can be obtained from the state dependence of the switching fields; for example we observe a systematic difference of $U_2^+(000)$ and $U_2^+(100)$ (Fig. 3c-d, see Supplementary Information). We stress here that the interaction strength necessary to obtain scrambling is directly proportional to the differences between the switching fields of different hysterons. Hence, as tilting allows to make these differences arbitrarily small near crossings, our strategy is eminently suited to observe non-Preisach behavior, even if hysteron interactions are weak. We conclude that hysteron interactions can yield novel types of pathways and t-graphs.

E. Strong interactions

To further study the effect of interaction between hysterons, we require samples with stronger coupling. To create these, we note that for typical parameters and $R \gtrsim 5$ cm, the (un)snapping of one hysteron triggers the (un)snapping of all hysterons, which we interpret as strong interactions, while for smaller R the snapping events occur in sequence. Exploring various samples, we observed that the radius of curvature is a proxy for the strength of interactions—the larger the radius, the stronger the interactions. We thus introduce sample C with $R = 2$ cm (the radius of curvature for sample A was 1 cm) and three grooves. We have verified that, in comparison to sample A, the interactions as measured by the dependence of the switching fields on the state are indeed stronger (see Supplementary Information). We orient the sample and apply a shim to the boundaries so that the crossings of the switching fields as function of α are optimally separated.

We find that, as a function of the tilt angle α , sample C yields nine distinct t-graphs, occurring on well-separated ranges of α (Fig. 4). We distinguish a number of distinct features. First, t-graphs $C(i)$, $C(ii)$, $C(iii)$ and $C(ix)$ are all Preisach graphs. Second, t-graphs $C(iv)$ and $C(v)$ feature an avalanche $\{100\} \rightarrow \{111\}$ over a significant range of tilt angles α . While we cannot rule out

that this avalanche is caused by inertial effects or degeneracies, we note the avalanche occurs over a significant range of α , and that hysteron interactions can also cause such avalanches; if $U_3^+(110) < U_2^+(100) < U_3^+(100)$, state $\{100\}$ transitions to $\{110\}$ at $\bar{U} = U_2^+(100)$, and since state $\{110\}$ is unstable at this value of U , it transitions to a stable state $\{111\}$. Third, t-graphs $C(v)$, $C(vi)$, $C(vii)$ and $C(viii)$ all contain scrambled transitions—see Table I for the pairs of scrambled transitions. Hence, manipulating the overall geometry of our corrugated sheets allows to increase the magnitude of interactions to obtain a variety of robust, non-Preisach pathways.

F. Memory effects

We now explore the range of distinct memory effects that occur in our samples due to hysteron interactions. We first note that the definition of ordinary return point memory (RPM)—when the driving strength revisits a previous extremal value, the system then revisits a previous extremal state [14, 15, 17, 27, 28]—does not have a one-to-one correspondence to the t-graph’s topology, and we therefore also consider a recent topological definition of *loop-RPM* (l-RPM) [13, 28]. l-RPM requires that all loops within the t-graph are absorbing. In essence, a loop is defined by a pair of nodes S_m and S_M , where the system evolves from S_m to S_M (and vice-versa) by a series of up (down) transitions, and the intermediate states are defined as the up (down) boundaries; l-RPM then requires states S_m (S_M) to be accessible by a sequence of down (up) transitions from any up (down) boundary.

All t-graphs of sample A, and all t-graphs of sample C—with the exception of $C(viii)$, which we will discuss in detail below—are consistent with l-RPM. We note that l-RPM graphs thus not only encompass Preisach graphs, but also t-graphs that are scrambled and/or feature avalanches.

What about ordinary RPM? RPM implies l-RPM, as all extremal states are absorbing states when RPM is valid [13]. The reverse however is not true: RPM implies conditions on the values of the switching fields beyond

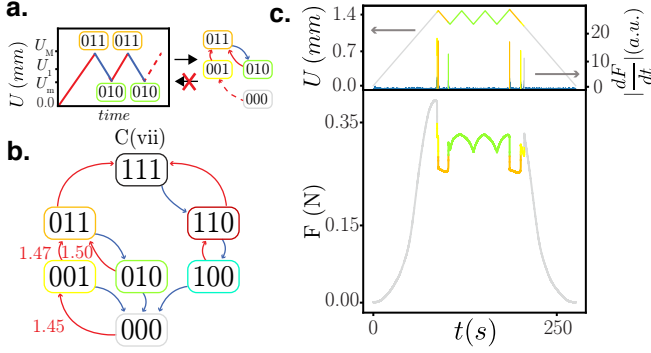


FIG. 5. **Breaking RPM.** **a**, While a strict RPM (left part) implies l-RPM (right part), l-RPM does not imply strict RPM. **b**, $C(vii)$ is a scrambled t-graph with l-RPM. However, as $U_2^+(001) < U_3^+(010)$ (indicated in mm), this pathway can violate RPM and satisfy l-RPM. **c**, Cycles between U_M , with $U_2^+(001) < U_M < U_3^+(010)$ (we take $U_M = 1.476$ mm) and $U_m > U_2^-(010)$ (we take $U_m = 1.210$ mm) leave the system in state $\{010\}$, despite U_M being larger than the critical up transition value of state $\{001\}$, thus breaking strict RPM. In the last cycle we increase U beyond $U_3^+(010) = 1.50$ mm and reach state $\{011\}$. Peaks of $|\frac{dF}{dt}(t)|$ indicate transitions

those captured by the topology of the t-graph: a system can be l-RPM without strictly satisfying RPM. To illustrate this, consider the scenario sketched in Fig. 5a. Here, state $\{011\}$ can be reached by up transitions from either $\{001\}$ which is part of the main loop or $\{010\}$ which is part of a secondary, nested loop. Consider a driving protocol where U is increased to a value U_M so that state $\{011\}$ is reached, then decreased to U_m so that state $\{010\}$ is reached, and then back up again to U_M . If the system satisfies RPM, it should revisit state $\{011\}$, and not remain stuck at state $\{010\}$, for any value of U_M that leads to state $\{011\}$ in the first up sweep of U . This implies a condition on the switching fields: $U_2^+(001) \geq U_3^+(010)$. In the absence of hysteron interactions, the switching fields are state independent, and the sequence of transitions on the main loop implies that $U_2^+ > U_3^+$, so that the above condition is satisfied. However, in the presence of hysteron interactions, the sequence of transitions on the main loop only implies that $U_2^+(000) > U_3^+(000)$ and $U_2^+(001) > U_3^+(000)$, but does not imply that $U_2^+(001) \geq U_3^+(010)$.

A specific example of a t-graph that follows this scenario and satisfies l-RPM but violates RPM is sample C in regime (vii) (Fig. 5b). When cycling the system (starting from $\{010\}$) between $U^M = 1.476$ mm and $U^m = 1.210$ mm, the system remains stuck in the $\{010\}$ state; only when U_M is increased beyond $U_3^+(010)$ does the system revisit state $\{011\}$ (Fig. 5c). Hence, sample $C(vii)$ does not satisfy ordinary RPM. Such (weak) breaking of RPM is a consequence of hysteron interactions, and our observations thus evidence distinct flavors of return point memory.

G. Accumulator pathway

We now revisit sample C in regime (viii). The loop that connects states $S_m = \{000\}$ and $S_M = \{011\}$ is not absorbing, as the up transitions from state $\{010\}$, part of the down boundary, never reaches S_M . Hence, hysteron interactions in this sample are sufficiently strong to break the hierarchical organization of loops-within-loops that characterizes t-graphs with the l-RPM property. We stress here that it is known that ferromagnetic interactions, where one hysteron switching from zero to one promotes the switching of others from zero to one and vice versa, preserve l-RPM[17]. Hence our observations directly evidence anti-ferromagnetic interactions, which clearly can cause a wide range of t-graphs [4]. To understand the new qualitative feature corresponding to this specific case we compare the response to cyclic driving in regime (vii), where the t-graph is l-RPM, and regime (viii), focussing on the loop that connects states $S_m = \{000\}$ and $S_M = \{011\}$ (Fig. 6a-d). In regime (vii), once the state $\{011\}$ is reached, cycling U between $U_m (> U_2^-(010))$ and $U_M (< U_1^+(011))$ the system follows the same $\{011\}$ - $\{010\}$ loop repeatedly (Fig. 6a,b). In contrast, applying a similar driving to the sample for α in regime (viii), yields state $\{011\}$ at first maximal driving, but the second and subsequent maxima produce state $\{110\}$ (Fig. 6c,d). Hence, the transition $\{010\} \rightarrow \{110\}$ “erases” the memory of the $\{011\}$ state and brings the system to a new sub-loop. This behavior, where the sample ‘remembers’ how often it is driven to a certain maximum is different from classical forms of memory [27] but rather can be seen as an elementary form of information processing: counting to two. We stress that this ‘accumulator’ behavior [29] can be observed on a robust range of tilt angles (see Fig. 4b).

t-graph	t_1	t_2
C(v)	$\{111\} \rightarrow \{101\}$	$\{011\} \rightarrow \{010\}$
C(vi)	$\{111\} \rightarrow \{101\}$	$\{011\} \rightarrow \{010\}$
C(vi)	$\{000\} \rightarrow \{001\}$	$\{100\} \rightarrow \{110\}$
C(vii)	$\{000\} \rightarrow \{001\}$	$\{100\} \rightarrow \{110\}$
C(viii)	$\{000\} \rightarrow \{001\}$	$\{100\} \rightarrow \{110\}$

TABLE I. Pairs of scrambled transitions (t_1, t_2) in Sample C.

II. CONCLUDING REMARKS

We presented a system with experimentally accessible mechanical hysterons which allows us to study emergent complex pathways. In particular, our work shows that hysteron interactions yield a plethora of essentially unexplored t-graphs, memory effects, and properties, such as strict RPM, l-RPM, scrambled pathways, avalanches and accumulator pathways. Moreover, we have shown that specific behaviors are not a only property of specific

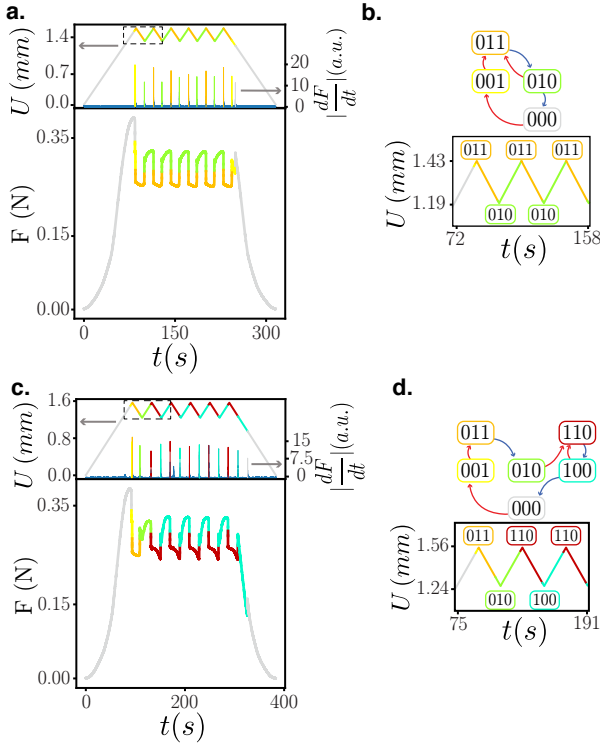


FIG. 6. **Accumulator behavior.** **a**, Repeated compression cycles yield repeated loops between the same extremal states (indicated by color) in regime (vii), consistent with RPM. Peaks of $|dF/dt(t)|$ indicate transitions. **b**, Corresponding pathway. **c**, Repeated compression cycles in regime (viii) evidence ‘accumulator’ behavior which violates RPM. **d**, Corresponding pathway where the first and subsequent extremal states are different.

samples but can be tuned geometrically and rationally via the boundaries.

Our work emphasizes the proliferation of complex t-graphs in complex media. Studies that explore t-graphs in such frustrated systems have just started to emerge and so far focus on numerics [5, 19, 20], and we hope our work motivates further studies by experiments as well. At present, we have little information about the statistics of different classes of t-graphs, the levels of complexity that can be reached and observed, and their relations to physical properties of the underlying system, all of which provide fertile ground for further study.

Our work further suggests to investigate the utility of complex t-graphs in rationally designed metamaterials. Finding strategies to arbitrarily control hysteron properties and their interactions, beyond the boundary control method introduced here, may open up a large design space for the rational design of pathways and t-graphs. Formally, the t-graphs have the same structure as the directed graphs that encode computations by finite state machines [30]. Hence, we suggest that a fruitful perspective on t-graphs in complex matter starts from their information processing capabilities. We note that while our systems are purely elastic and thus microscopically re-

versible, one imagines that material plasticity will lead to evolution of such pathways, which perhaps can be used to train materials to exhibit targeted pathways. Together, such control, design and learning strategies can be explored, in particular in systems with many hysterons, to achieve mechanical systems which, in response to external driving, process complex information.

ACKNOWLEDGMENTS

We gratefully acknowledge discussions with C. Coulais, M. Mungan, E. Verhagen, N. Keim and J. Paulsen.

Appendix A: Methods

1. Sample fabrication and experimental protocol

The fabrication of corrugated sheets starts by spin coating a liquid mixture of a two components silicone elastomer (Zhermack Elite double 32 Fast, Young’s modulus $E \approx 1$ MPa, Poisson’s ratio $\nu \approx 0.5$) on a surface with sinusoidal corrugations with pitch p and amplitude A_0 . Rotation is maintained until complete curing of the polymer (≈ 20 min). The sheet is then peeled and rolled in an open cylinder; top and bottom ends are dipped in a liquid layer of the same polymer mixture to set the cylindrical shape and fix the boundary conditions. The resulting sample is characterized by its height H , thickness t , radius of curvature R , pitch p and number of corrugations N , and amplitude A_0 . Paint is splattered on the samples to enhance contrast and ease visualization.

The mechanical response of our samples is probed in a uniaxial testing device (Instron 3366) which controls the axial compression U better than $10 \mu\text{m}$; we use a 5N sensor which accurately measures the force down to 10 mN with an accuracy of 10^{-4} N. We define $U = 0$ where the force during compression reaches the small value $F(U_0) = 20$ mN. We use compression speeds of 1 mm/min and have checked that further lowering the compression speed by an order of magnitude does not affect the phenomenology, thus ensuring we operate in the quasistatic regime. We focus on the compression range (strain less than 5%) where grooves can snap but where no additional instabilities are observed.

We image the deformation of the groovy sheet during compression at a frame rate of 3Hz or faster, using a CCD camera (Basler acA2040-90um) mounted with a 50 mm objective. We calculate the mean squared differences in each local region Ω_i of the normalized digital image as: $\sum_{k,l \in \Omega_i} \Delta_i^2 k,l := (A_{k,l}^{t+\Delta t} - A_{k,l}^t)^2$, where k and l label the pixels, t is time, and Δt the time interval ($\Delta t = 100$ ms in Fig. 1e). Each region Ω_i targets a part of a single groove, chosen such that events in neighbouring regions do not create secondary peaks.

The sample rests on a Thorlabs tilt stage that allows to control the tilt angle α with an accuracy of

3.10^{-5} rad. We incrementally change α with steps ranging from 3.10^{-4} rad to 2.10^{-3} rad, and for each tilt angle α measure the full t-graph and the mechanical response. All transition graphs presented in this paper were obtained multiple times over the course of several weeks, and all angles were visited several times to ensure a good reproducibility (see Supplementary Fig. S1c,d). By exploring the reproducibility of the boundary between different t-graphs, when two switching fields are essentially degenerate, we estimate our accuracy of the boundaries to be better than $\pm 2.10^{-4}$ rad.

To determine the switching fields, each transition is probed between two and four times, and we report mean switching fields which have a standard deviation typically smaller than the symbol-size. We estimate small viscous relaxation effects to affect the switching field by at most 4% (Supplementary Fig. S1b), thus requiring larger differences to evidence interactions.

Appendix B: Supplementary Material

1. Supplementary Videos 1, 2 and 3

Front view of sample A during a compression/decompression cycle presenting the main loop for three increasing values of the tilt angle α . These three movies demonstrate how the order of snapping and unsnapping events is modified by the tilt angle: supplementary movie 1 corresponds to topology A(i), supplementary movie 2 to A(vi) and supplementary movie 3 to A(vii). The compression speed is 5 mm/min, the movies were recorded at a frame rate of 24Hz, and are real time.

2. Reproducibility, plasticity and ageing

We performed 150 compression cycles on sample A, where each driving sub-cycle (Fig. 1i, inset) is repeated 50 times, and observe a very good reproducibility of the pathways and response (Supplementary Fig. 7a). We also monitored the force relaxation under large compression, and find a force decay of approximately 7% over three hours (Supplementary Fig. 7b). We estimate the amount of relaxation during typical experiments (compression is close to the maximum for approximately 1 min) to be on the order of 4%. While such relaxation has a minor impact on the exact values of the switching fields, it does not influence the topology of the t-graphs. Moreover, such relaxation is fully reversible after releasing the load, and long-term plastic ageing of the sample is essentially absent: the data presented in this paper were acquired over the course of many months, with no visible changes in the mechanical response. Similarly, we emphasize the high reproducibility of the mechanical response when a

tilt angle is revisited, and have been able to easily reproduce the full response in such cases (Supplementary Fig. 7c-d).

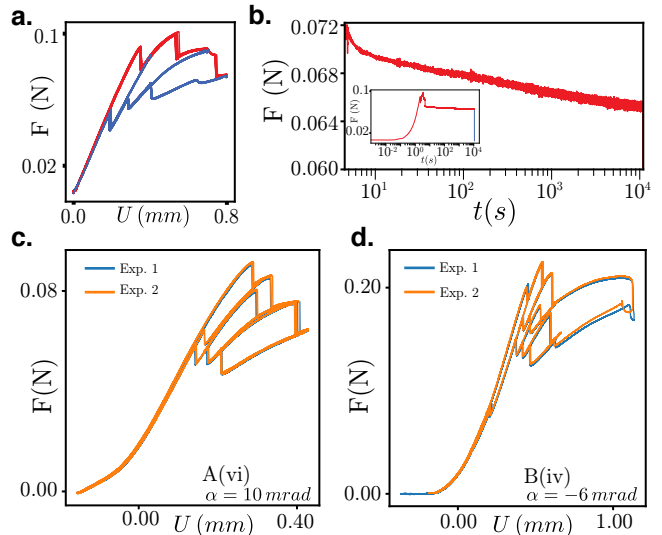


FIG. 7. **a**, 150 cycles of compression performed on sample A (protocol similar as inset of Fig. 1i, where each sub-cycle is repeated 50 times). Deformation pathways reproduce. **b**, Force relaxation of sample A. Compression is maintained at $U = 0.8$ mm for three hours, the force relaxes by approximately 7%, with no creeping effect. Inset: full signal **c,d** When a tilt angle α is revisited, the mechanical response reproduces (**c**: sample A; **d**: sample B).

3. Sample B.

We perform a systematic tilting experiment with the four grooves sample B, whose other geometrical parameters are close to sample A (Supplementary Fig. 8). We obtained nine t-graphs, eight of which are Preisach, and one is scrambled (Supplementary Fig. 8a1, a2). Similar to sample A (Fig. 2), most changes in the topology of the t-graphs are associated with a single permutation of P^+ or P^- (Supplementary Fig. 8a1, a2). We attribute the $B(i)$ to $B(ii)$ and $B(vi)$ to $B(vii)$ cases, that involve two permutations, to the near degeneracy of two t-graph transitions. A close inspection of the switching fields reveals that a change in the t-graphs topology coincides with the crossing of the relevant switching fields (Supplementary Fig. 9b1,b2). Finally, despite the very weak interactions (as seen by the very small state dependence of the various switching fields, Supplementary Fig. 9b1,b2), we found a t-graph B(v) whose transitions $\{1111\} \rightarrow \{1011\}$ and $\{0111\} \rightarrow \{0101\}$ are scrambled. B(v) exists on a very narrow angle range (Supplementary Fig. 8b), where the relevant switching fields are quite close, but we nevertheless have been able to reproduce it several times.

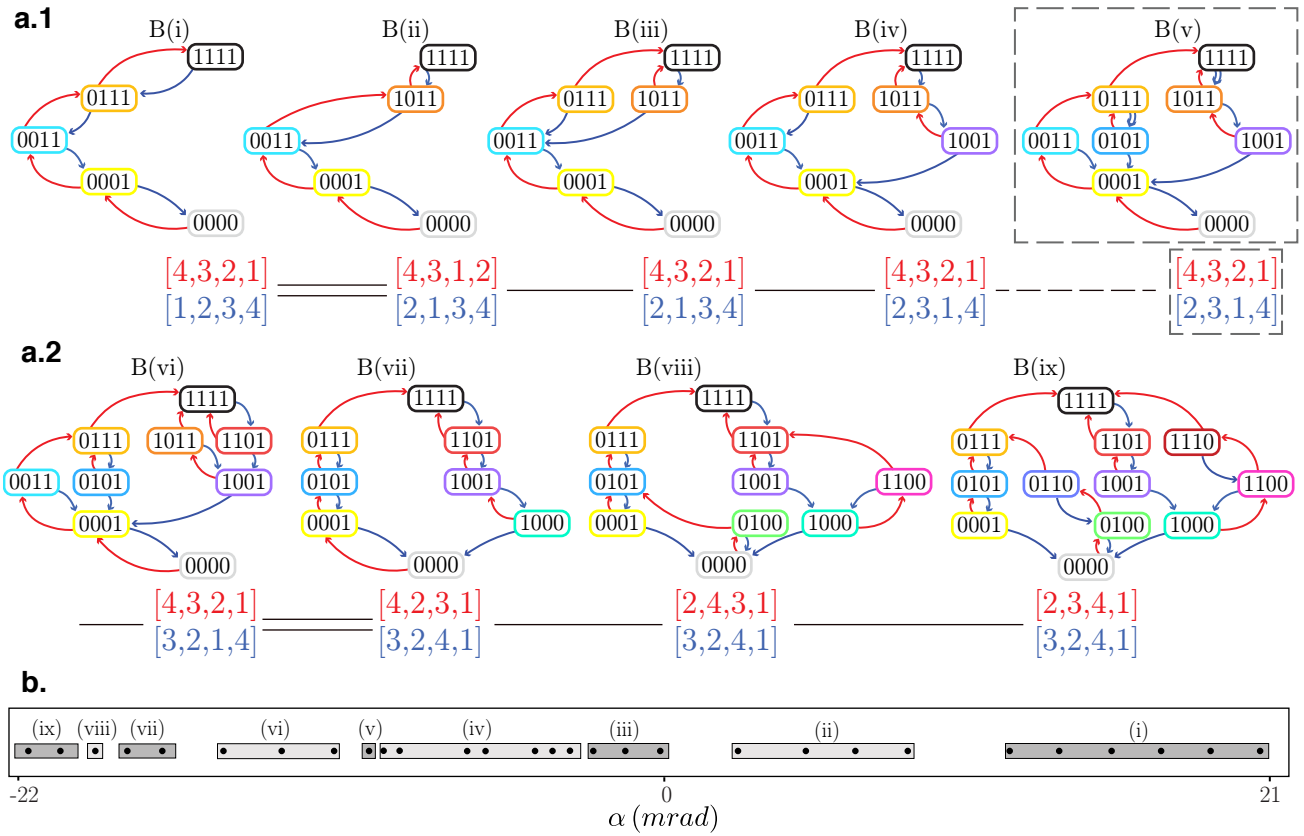


FIG. 8. **Tunable Preisach transition graphs (sample B).** **a1,2**, Tilting the bottom boundary of sample B ($\{H, t, R, p, A_0\} = \{30, 0.3, 1.0, 8, 3\}$ mm and $N = 4$ corrugations) elicits nine Preisach t-graphs and one scrambled t-graphs (dashed box), where the scrambled transitions are shown by double arrows. The red (blue) lists indicate the order of the up (down) transitions of the main loop P^+ (P^-). The angle α increases monotonically from B(ix) to B(i) **b**, t-graph as function of the tilt angle α .

4. Switching fields.

Figure 9 presents the different switching fields as a function of the tilt angle α , for all samples presented in the paper.

-
- [1] J. D. Paulsen, N. C. Keim, and S. R. Nagel, Multiple transient memories in experiments on sheared non-brownian suspensions, *Phys. Rev. Lett.* **113**, 068301 (2014).
 - [2] N. C. Keim, J. Hass, B. Kroger, and D. Wieker, Global memory from local hysteresis in an amorphous solid, *Phys. Rev. Research* **2**, 012004 (2020).
 - [3] M. Adhikari and S. Sastry, Memory formation in cyclically deformed amorphous solids and sphere assemblies, *The European Physical Journal E* **41**, 105 (2018).
 - [4] M. Mungan, S. Sastry, K. Dahmen, and I. Regev, Networks and hierarchies: How amorphous materials learn to remember, *Phys. Rev. Lett.* **123**, 178002 (2019).
 - [5] I. Regev, I. Attia, K. Dahmen, S. Sastry, and M. Mungan, The topology of the energy landscape of sheared amorphous solids and the irreversibility transition (2021), arXiv:2101.01083 [cond-mat.soft].
 - [6] K. Matan, R. B. Williams, T. A. Witten, and S. R. Nagel, Crumpling a thin sheet, *Phys. Rev. Lett.* **88**, 076101 (2002).
 - [7] Y. Lahini, O. Gottesman, A. Amir, and S. M. Rubinstein, Nonmonotonic aging and memory retention in disordered mechanical systems, *Phys. Rev. Lett.* **118**, 085501 (2017).
 - [8] F. Preisach, Über die magnetische nachwirkung, *Zeitschrift für Physik* **94**, 277 (1935).
 - [9] M. Serra-Garcia, Turing-complete mechanical processor via automated nonlinear system design, *Phys. Rev. E* **100**, 042202 (2019).
 - [10] Y. Song, R. M. Panas, S. Chizari, L. A. Shaw, J. A. Jackson, J. B. Hopkins, and A. J. Pascall, Additively manu-

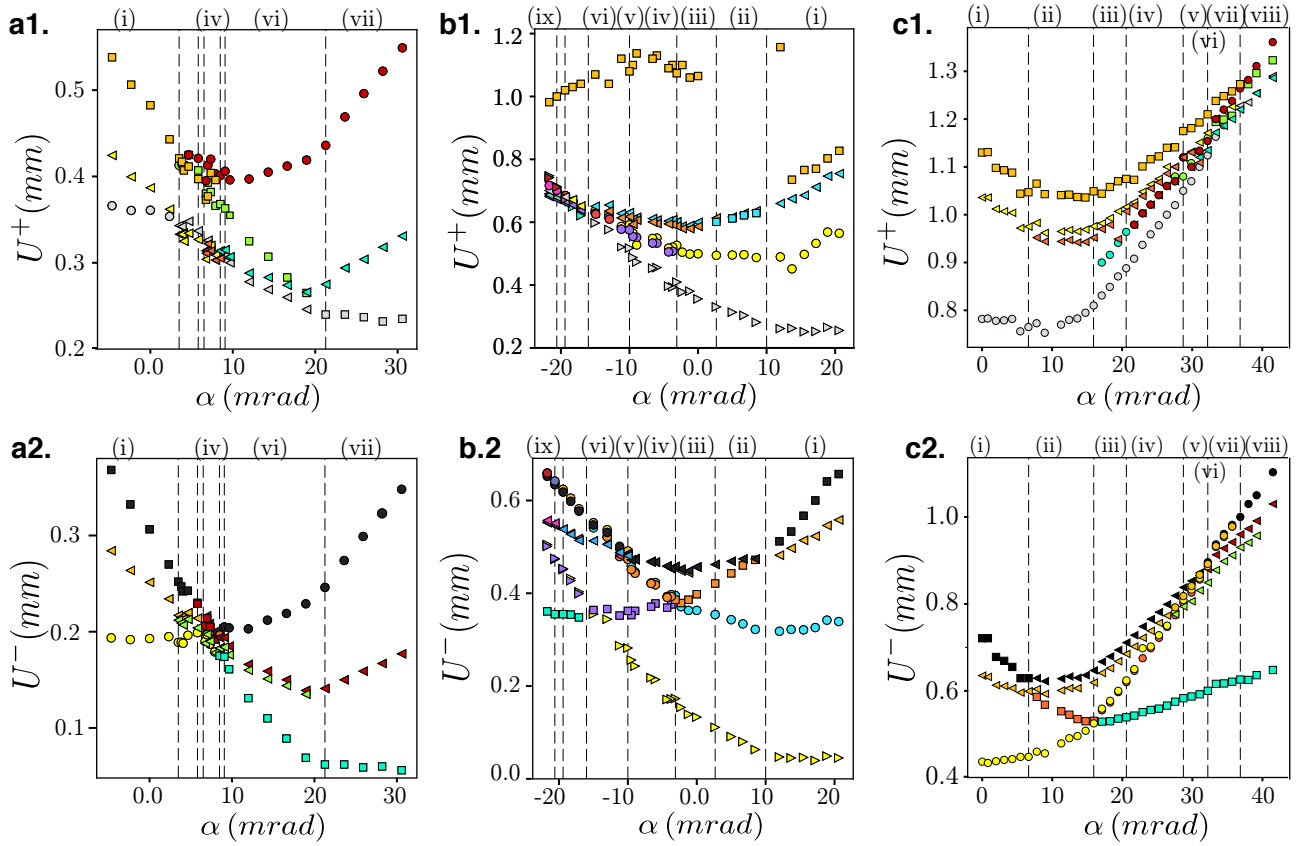


FIG. 9. **Switching fields.** U^+ and U^- as a function of the tilt angle α (a: sample A, b: sample B, c: sample C). Symbols refer to hysteron 1 (\square), 2 (\triangle), 3 (\circ) or 4 (\triangleright); colors refer to the state. For example, a yellow circle in panel (b1) shows $U_3^+(0001)$. Dotted lines mark the boundaries between network topologies, with some narrow ranges not labeled for legibility.

- facturable micro-mechanical logic gates, *Nature Communications* **10**, 882 (2019).
- [11] T. Chen, M. Pauly, and P. M. Reis, A reprogrammable mechanical metamaterial with stable memory, *Nature* **589**, 386 (2021).
- [12] J. D. Paulsen and N. C. Keim, Minimal descriptions of cyclic memories, *Proceedings of the Royal Society A: Mathematical, Physical and Engineering Sciences* **475**, 20180874 (2019), <https://royalsocietypublishing.org/doi/pdf/10.1098/rspa.2018.0874>.
- [13] M. Mungan and M. M. Terzi, The structure of state transition graphs in systems with return point memory: I. general theory, *Annales Henri Poincaré* **20**, 2819 (2019).
- [14] J. A. Barker, D. E. Schreiber, B. G. Huth, and D. H. Everett, Magnetic hysteresis and minor loops: models and experiments, *Proceedings of the Royal Society of London. A. Mathematical and Physical Sciences* **386**, 251 (1983), <https://royalsocietypublishing.org/doi/pdf/10.1098/rspa.1983.0035>.
- [15] D. H. Everett and W. I. Whitton, A general approach to hysteresis, *Trans. Faraday Soc.* **48**, 749 (1952).
- [16] J. M. Deutsch, A. Dhar, and O. Narayan, Return to return point memory, *Phys. Rev. Lett.* **92**, 227203 (2004).
- [17] J. P. Sethna, K. Dahmen, S. Kartha, J. A. Krumhansl, B. W. Roberts, and J. D. Shore, Hysteresis and hierarchies: Dynamics of disorder-driven first-order phase transformations, *Phys. Rev. Lett.* **70**, 3347 (1993).
- [18] O. Hovorka and G. Friedman, Onset of reptations and critical hysteretic behavior in disordered systems, *Journal of Magnetism and Magnetic Materials* **290-291**, 449 (2005), proceedings of the Joint European Magnetic Symposia (JEMS' 04).
- [19] C. W. Lindeman and S. R. Nagel, Multiple memory formation in glassy landscapes (2021), arXiv:2101.01632 [cond-mat.soft].
- [20] N. C. Keim and J. D. Paulsen, Multiperiodic orbits from interacting soft spots in cyclically-sheared amorphous solids (2021), arXiv:2101.01240 [cond-mat.soft].
- [21] R. F. Shepherd, F. Ilievski, W. Choi, S. A. Morin, A. A. Stokes, A. D. Mazzeo, X. Chen, M. Wang, and G. M. Whitesides, Multigait soft robot, *Proceedings of the National Academy of Sciences* **108**, 20400 (2011), <https://www.pnas.org/content/108/51/20400.full.pdf>.
- [22] J. T. B. Overvelde, T. Kloeck, J. J. A. D'haen, and K. Bertoldi, Amplifying the response of soft actuators by harnessing snap-through instabilities, *Proceedings of the National Academy of Sciences* **112**, 10863 (2015), <https://www.pnas.org/content/112/35/10863.full.pdf>.
- [23] M. Wehner, R. L. Truby, D. J. Fitzgerald, B. Mosadegh, G. M. Whitesides, J. A. Lewis, and R. J. Wood, An integrated design and fabrication strategy for entirely soft, autonomous robots, *Nature* **536**, 451 (2016).
- [24] C. Coullais, A. Sabbadini, F. Vink, and M. van Hecke, Multi-step self-guided pathways for shape-changing

- metamaterials, *Nature* **561**, 512 (2018).
- [25] M. A. McEvoy and N. Correll, Materials that couple sensing, actuation, computation, and communication, *Science* **347**, 10.1126/science.1261689 (2015), <https://science.sciencemag.org/content/347/6228/1261689.full>.
- [26] S. Bourgeois, B. Cochelin, F. Guinot, and E. Picault, Buckling analysis of tape springs using a rod model with flexible cross-sections, *European Journal of Computational Mechanics* **21**, 184 (2012), <https://doi.org/10.1080/17797179.2012.714848>.
- [27] N. C. Keim, J. D. Paulsen, Z. Zeravcic, S. Sastry, and S. R. Nagel, Memory formation in matter, *Rev. Mod. Phys.* **91**, 035002 (2019).
- [28] M. M. Terzi and M. Mungan, State transition graph of the preisach model and the role of return-point memory, *Phys. Rev. E* **102**, 012122 (2020).
- [29] A. Schurger, J. D. Sitt, and S. Dehaene, An accumulator model for spontaneous neural activity prior to self-initiated movement, *Proceedings of the National Academy of Sciences* **109**, E2904 (2012), <https://www.pnas.org/content/109/42/E2904.full.pdf>.
- [30] J. Sakavorith, *Elements of automata theory* (Cambridge University Press, London, 2009).